

study as much as possible to questions of electrical structure.

#### ACKNOWLEDGMENTS

We wish to express our sincere thanks to Dr. R. L. Petritz for having stimulated our interest in PbS films

and for several helpful discussions throughout the course of this work. In addition, we wish to thank Dr. R. F. Brebrick of the U. S. Naval Ordnance Laboratory and Dr. Harry E. Spencer of Eastman-Kodak for generously furnishing the samples used in this investigation.

### Microwave Faraday Effect in Silicon and Germanium\*

J. K. FURDYNA

*Northwestern University, Evanston, Illinois*

AND

S. BROERSMA

*University of Oklahoma, Norman, Oklahoma*

(Received August 1, 1960; revised manuscript received September 7, 1960)

The Faraday rotation and ellipticity in a system of quasifree carriers is discussed and applied to microwave measurements on semiconductors. The theoretical expressions for these effects are analyzed with a digital computer for various ranges of the magnetic field  $B$ , the mobility  $\mu$ , the conductivity  $\sigma$ , the frequency  $\omega$ , the collision time  $\tau$  and the dielectric constant of the host material. It is possible to simplify these expressions in certain limiting cases. For  $\mu B$  smaller than unity, the rotation and ellipticity are proportional to  $B$ . For  $\mu B$  larger than both unity and  $\omega\tau$ , they decrease as  $B^{-1}$  and  $B^{-3}$ , respectively. A maximum occurs near  $\mu B = 1$  when  $\omega\tau$  is small.

Rotation measurements on  $n$ - and  $p$ -type single crystals of silicon at room temperature, with resistivities from 0.5 to 40 ohm-cm, utilizing 9.6- and 35-kMc/sec radiation, are compared with the theory. Results for  $n$ -type germanium at 78°K, with  $\mu B$  varied up to about 6, agree with the calculated low- and high-field behavior. Faraday ellipticity measurements on  $n$ -type germanium crystals at 78°K are in qualitative agreement with the theory. In the case of small losses, the sign of the ellipticity is determined by the sign of the quantity  $(4\omega\tau - \sigma/\omega\epsilon_{st})$ .

#### A. INTRODUCTION

THE Faraday effect in a longitudinally magnetized substance can be observed as a rotation and as an elliptical polarization of an initially plane polarized wave. Here the theoretical equations will be compared with the experimental results obtained for various semiconductor samples for a broad range of conductivities.

The complex propagation constants for the left- and right-circularly polarized electric field components of a traveling electromagnetic wave (indicated by  $+$  and  $-$ , respectively) can be written<sup>1,2</sup>

$$k_{\pm}^2 \equiv (\alpha_{\pm} \mp i\beta_{\pm})^2 = \mu_0\omega^2(\epsilon_{\pm}' \mp i\epsilon_{\pm}''), \quad (1)$$

where  $\mu_0$  is the permeability of free space,  $\omega$  the microwave angular frequency, and  $\epsilon_{\pm}'$  and  $\epsilon_{\pm}''$  the real and imaginary parts of the effective dielectric constant of the medium, all in mks units.

Using the one-carrier model for semiconductors, one

can write

$$\epsilon_{\pm}' = \epsilon_{st}' - \frac{\sigma/\omega(\omega\tau \pm \mu B)}{1 + (\omega\tau \pm \mu B)^2}, \quad \epsilon_{\pm}'' = \frac{\sigma/\omega}{1 + (\omega\tau \pm \mu B)^2}, \quad (2)$$

where  $\epsilon_{st}'$  is the dielectric constant of the host material,  $\sigma$  the dc conductivity at  $B=0$ ,  $\mu = q\tau/m^*$  the carrier mobility,  $\tau$  the effective time between collisions,  $m^*$  the effective mass of the charge carriers,  $q$  the carrier charge, and  $B$  the dc magnetic field.

From Eq. (1) the propagation constants are readily found to be

$$(\alpha_{\pm}, \beta_{\pm}) = \omega(\mu_0/2)^{1/2} [(\epsilon_{\pm}'^2 + \epsilon_{\pm}''^2)^{1/2} (+, -) \epsilon_{\pm}']^{1/2}. \quad (3)$$

The angle  $\theta$  through which the plane of polarization rotates as the wave progresses a distance  $l$  in the medium then is given by

$$\theta = \frac{1}{2}(\alpha_- - \alpha_+)l \text{ radians}. \quad (4)$$

Similarly, the ellipticity, i.e., the ratio of the minor to the major axis of the resulting electric field pattern, is

$$E = \tanh\left[\frac{1}{2}(\beta_- - \beta_+)l\right] \approx \frac{1}{2}(\beta_- - \beta_+)l. \quad (5)$$

On the basis of this model Rau and Caspari were able to discuss successfully their measurements on  $n$ -

\* This work was supported by the National Science Foundation. (J. K. Furdyna, Thesis, Northwestern University, Evanston, Illinois, May 1960).

<sup>1</sup> R. R. Rau and M. E. Caspari, Phys. Rev. **100**, 632 (1955).

<sup>2</sup> M. J. Stephen and A. B. Lidiard, J. Phys. Chem. Solids **9**, 43 (1959).

and *p*-type germanium crystals with resistivities of about 15 ohm-cm. Thus, applying Eqs. (2) to (4) to gray tin, the present authors expected to see large effects in this material, even for very thin samples. However, an experiment with gray tin in both single-crystal and powder form (carrier concentration at 78°K: 10<sup>17</sup> per cm<sup>3</sup> and higher) revealed that the effect, if any, was less than 0.1°. The experiment was carried out at 78°K and 300°K in fields up to 0.4 v-sec/m<sup>2</sup> (4 kilogauss), with 10- and 35-kMc/sec radiation, on crystal samples about 0.2 mm thick or on comparable quantities of powder. This lack of agreement prompted a further investigation of the applicability of the theory to silicon and germanium at impurity concentrations higher than those already discussed in the literature.

As an interesting by-product of the gray tin experiment, it was observed at 78°K that the transmission through single crystals oscillated in time in certain instances. The gray tin samples were soldered with mercury to a waveguide diaphragm. The phenomenon appeared spontaneously, was rather unstable and disappeared upon slight changes in the ambient conditions (rise of temperature, sample displacement, etc.). The frequency of the observed oscillations ranged between 0.5 and 3 cps, with a maximum-to-minimum ratio of the transmitted power usually larger than 2. The waveform and frequency of the oscillations were sensitive to the magnetic field. In some respects the phenomenon resembles the "oscillistor" effect recently reported.<sup>3</sup>

**B. THEORETICAL DETAILS**

**Rotation**

In the range of  $\mu B$  smaller than 1 and in low-loss materials, i.e., when  $\epsilon'' < \epsilon'$ , the expression for  $\theta$  can be reduced to

$$\theta = \frac{1}{2} \left( \frac{\mu_0}{\epsilon_{st}'} \right)^{\frac{1}{2}} \sigma \mu B t \frac{1 - \omega^2 \tau^2}{(1 + \omega^2 \tau^2)^2} \tag{6}$$

For large losses, i.e.,  $\epsilon' < \epsilon''$ , the rotation can be approximated by

$$\theta = \frac{1}{2} \left( \frac{\mu_0 \omega \sigma}{2} \right)^{\frac{1}{2}} \mu B t \frac{1 + 2\omega\tau - \omega^2\tau^2}{(1 + \omega^2\tau^2)^{\frac{3}{2}}} \tag{7}$$

Evidently, at small values of  $\mu B$ , the Verdet constant  $V = \theta/Bt$  is a useful concept. Equation (6), without the  $\omega\tau$  factor was first given by Rau and Caspari.<sup>1</sup> Stephen and Lidiard<sup>2</sup> give an equation resembling Eq. (7), with  $\mu$  replaced by  $\mu_H$  (Hall mobility) for all types of energy surfaces.

In Fig. 1 these limiting equations are compared with the exact calculations. The circles represent the rota-

tions as obtained with a digital computer using Eqs. (2) to (4). In this computation only  $\sigma$  is varied, other parameters remaining constant:  $\epsilon_{st}'/\epsilon_0 = 12$ ,  $\omega = 2.2 \times 10^{11}$  cps,  $\tau = 2.6 \times 10^{-13}$  sec,  $\mu = 0.15$  m<sup>2</sup>/v-sec. Thus the dependence of  $\theta$  upon  $\sigma/\omega\epsilon_{st}'$  in the region of low and high losses is brought out clearly. The solid lines in Fig. 1 represent the approximate equations (6) and (7), without the  $\omega\tau$  factor. Using the complete Eq. (7) the dashed line is obtained.

In the region where  $\mu B$  is greater than both 1 and  $\omega\tau$ , the rotation decreases with  $B$ . Unlike the low-field behavior, the rotation is now rather insensitive to  $\tau$  (see the middle curve in Fig. 2), and thus unsuitable for the study of  $\tau$  or  $m^*$ . In the case  $\mu B > \sigma/\omega\epsilon_{st}'$ , the expression for  $\theta$  simplifies for any  $\omega\tau$  to

$$\theta = \frac{1}{2} \left( \frac{\mu_0}{\epsilon_{st}'} \right)^{\frac{1}{2}} \frac{\sigma \mu B t}{\mu^2 B^2 - \omega^2 \tau^2} \approx \frac{1}{2} \left( \frac{\mu_0}{\epsilon_{st}'} \right)^{\frac{1}{2}} \frac{n q t}{\mu B} \tag{8}$$

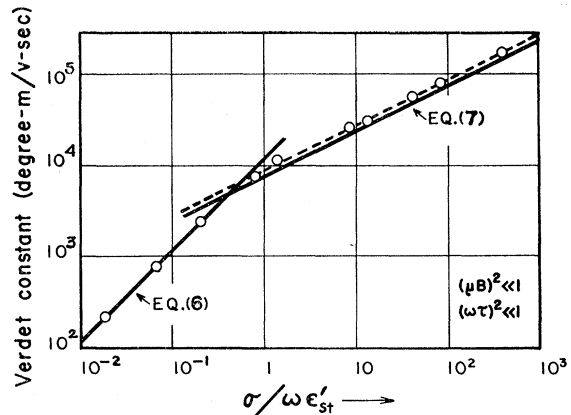


FIG. 1. Comparison of computer calculations with approximate formulas for the Verdet constant of a semiconductor as a function of the conductivity. The circles represent exact solutions of Eqs. (2) to (4), obtained for  $\omega = 2.2 \times 10^{11}$  cps,  $\mu = 0.15$  m<sup>2</sup>/v-sec,  $\tau = 2.6 \times 10^{-13}$  sec, and  $\epsilon_{st}'/\epsilon_0 = 12$ . The solid lines represent Eqs. (6) and (7) without the  $\omega\tau$  factor. The complete Eq. (7) gives the dashed line.

Here  $n$  is the charge carrier density. The values obtained from Eq. (8) agree within a few percent with the exact computer calculations for  $\omega\tau$  ranging from 0 to 1, and  $\mu B \geq 5$ . Note also the slope of  $-1$  in the high-field region of Fig. 2. Evidently, a high-field measurement can give the carrier concentration even if  $\sigma$  and  $\tau$  are not known. At magnetic fields such that  $\mu B > \sigma/\omega\epsilon_{st}'$ , it can be used to measure  $\epsilon_{st}'$  in samples of relatively high  $\sigma$ , for which the rotation shows little dependence on the dielectric constant at low magnetic fields, see Eq. (7).

Figure 2 indicates that the exact position of the maximum is not very sensitive to the magnitude of  $\sigma/\omega\epsilon_{st}'$  and  $\omega\tau$ , and may be written as

$$\mu B(\theta_{\max}) = 1.4 \pm 0.4 \tag{9}$$

over a wide range of these parameters. This can also easily be checked analytically. Hence, even an approximate knowledge of  $\sigma$  and  $\tau$  will permit a rather precise

<sup>3</sup> R. D. Larrabee and M. C. Steele, Bull. Am. Phys. Soc. 4, 421 (1959); I. L. Ivanov and S. M. Ryvkin, J. Tech. Phys. U.S.S.R. 28, 774 (1958) [translation: Soviet Phys.-Tech. Phys. 3, 722 (1958)].

determination of  $\mu B(\theta_{\max})$  for a given sample. Conversely, by locating such a maximum in the  $\theta$  vs  $B$  plot, one can estimate the carrier mobility in materials of unknown  $\sigma$ ,  $\tau$ ,  $\epsilon_{st}'$ , or thickness (powder samples).

Suhl and Walker,<sup>4</sup> among others, considered the rotation of the *guided* waves. According to them, if  $V$  is the Verdet constant in the unbounded medium, then for the  $TE_{11}$  mode traveling through a semiconductor,

$$V_g = 2\lambda_g V / 2.38\lambda_0 = 0.84V\lambda_g/\lambda_0,$$

where  $\lambda_g$  and  $\lambda_0$  are the wavelengths of the guided and the unbounded waves in the medium, respectively, and  $V_g$  the observed Verdet constant for the guided wave. Because of the large refractive index of silicon and germanium,  $\lambda_g \approx \lambda_0$ , so that

$$\theta_g \approx 0.84\theta = 0.84 \times \frac{1}{2}(\alpha_- - \alpha_+)l. \quad (10)$$

The above treatment does not hold near cutoff or for very high losses in the sample.

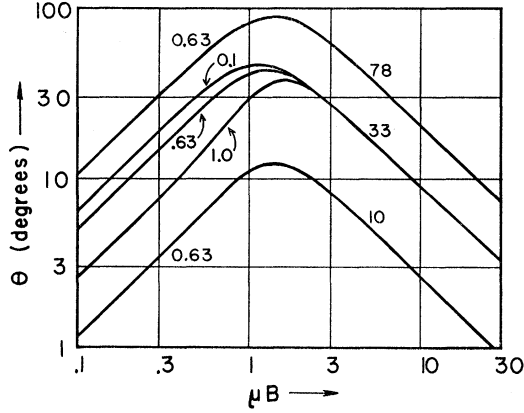


FIG. 2. Rotation as a function of  $\mu B$  at 35 kMc/sec. Curves are calculated using Eqs. (2) to (4), with  $\epsilon_{st}'/\epsilon_0 = 16$  and  $l = 1$  mm. The parameters  $\sigma$  (in  $\text{ohm}^{-1}\text{m}^{-1}$ ) and  $\omega\tau$  are indicated for each curve in the high- and low-field region of the graph, respectively.

### Ellipticity

It is convenient to consider ellipticity in the limit of small and large losses. For the case of *small losses*  $\epsilon'' < \epsilon'$ , and  $\mu B < 1$ , Eqs. (2), (3), and (5) give

$$E = \frac{1}{4} \left( \frac{\mu_0}{\epsilon_{st}'} \right)^{\frac{1}{2}} \frac{\sigma \mu B l}{(1 + \omega^2 \tau^2)^2} \left[ 4\omega\tau - \frac{\sigma}{\omega \epsilon_{st}'} \frac{1 - 3\omega^2 \tau^2}{1 + \omega^2 \tau^2} \right]. \quad (11)$$

Hence, for a *small* magnetic field the effect is proportional to  $\mu B$ . Equation (11) differs from the formula developed by Rau and Caspari<sup>1</sup> by the presence of the second term in the brackets. We retain this term because  $\omega\tau$  is small for semiconductors at ordinary temperatures. Evidently, the Faraday ellipticity reverses its sign at  $\omega^2 = \sigma/4\tau\epsilon_{st}' = nq^2/4m^*\epsilon_{st}'$ , i.e., when the microwave frequency equals half the classical plasma frequency; see also Fig. 3.

<sup>4</sup> H. Suhl and L. R. Walker, Phys. Rev. **86**, 122 (1952).

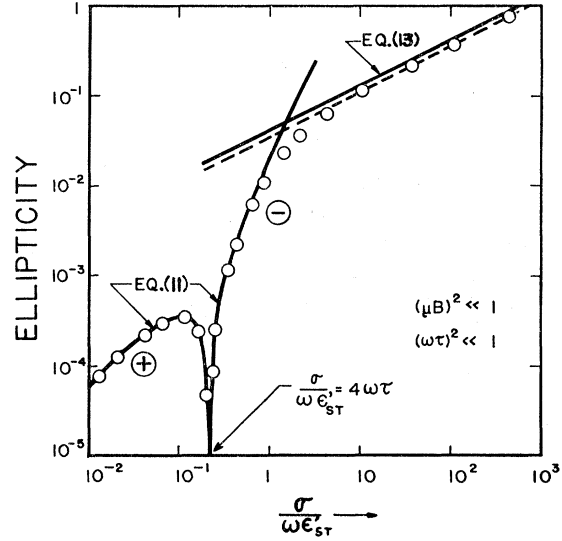


FIG. 3. Comparison of computer calculations with approximate formulas for the Faraday ellipticity in a semiconductor as a function of the conductivity  $\sigma$ . The circles represent exact solutions of Eqs. (2) to (5), obtained for  $\omega = 2.2 \times 10^{11}$  cps,  $\tau = 2.6 \times 10^{-13}$  sec,  $\mu = 0.15$  m<sup>2</sup>/v-sec,  $B = 0.30$  v-sec/m<sup>2</sup>,  $\epsilon_{st}'/\epsilon_0 = 12$ , and  $l = 1$  mm. The solid lines represent Eqs. (11) and (13) without the  $\omega\tau$  factor. The complete Eq. (13) gives the dashed line.

For *large* magnetic field strength the Faraday ellipticity can be expressed as

$$E = -\frac{1}{4} \left( \frac{\mu_0}{\epsilon_{st}'} \right)^{\frac{1}{2}} \frac{\sigma \mu B l}{(\mu^2 B^2 - \omega^2 \tau^2)^2} \times \left[ 4\omega\tau - \frac{\sigma}{\omega \epsilon_{st}'} \frac{\mu^2 B^2 + 3\omega^2 \tau^2}{\mu^2 B^2 - \omega^2 \tau^2} \right]. \quad (12)$$

It is interesting that the bracketed term resembles that of Eq. (11). Hence, at high fields it should also be possible to observe an ellipticity node as a function of  $n$  or  $\omega$ .

The rapid decrease of the ellipticity with the magnetic field may be important in a measurement of the rotation. This falls off at a slower rate. When the ellipticity is large, a rotation measurement is difficult. However, according to Eq. (12) the major axis of the ellipse can be defined sharply by increasing the field strength sufficiently.

The dependence of the ellipticity upon the field strength with  $\omega\tau$  as a parameter is illustrated in Fig. 4. An ellipticity *maximum* is observed near  $\mu B = 1$ . This maximum is sharper than the corresponding maximum in the rotation, and in general occurs at a somewhat lower field.

The equations for *large losses* are developed by neglecting  $(\epsilon''/\epsilon')^2$ . At *small* magnetic fields, the Faraday ellipticity is approximated by

$$E = -\frac{1}{2} \left( \frac{\mu_0 \omega \sigma}{2} \right)^{\frac{1}{2}} \mu B l \frac{1 - 2\omega\tau - \omega^2 \tau^2}{(1 + \omega^2 \tau^2)^{\frac{3}{2}}}. \quad (13)$$

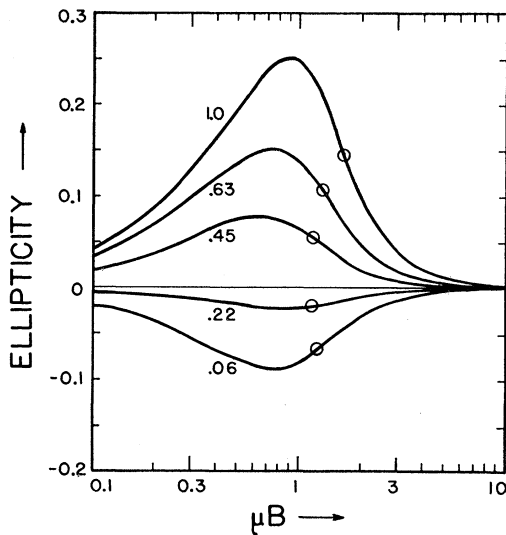


FIG. 4. Ellipticity as a function of  $\mu B$  at 35 kMc/sec. The curves are calculated with Eqs. (2) to (5), using  $\epsilon_{si}'/\epsilon_0=16$ ,  $\sigma=33$  ohm $^{-1}$  m $^{-1}$ ,  $l=0.5$  mm, and the values of  $\omega\tau$  as indicated in the graph. The behavior shown is characteristic of low-loss materials. Note that  $(4\omega\tau - \sigma/\omega\epsilon_{si}')$  determines the sign. The circles mark the positions at which the corresponding rotation maxima occur.

Thus a change of sign occurs near  $\omega\tau=0.4$ . The exact condition for zero ellipticity depends upon  $\epsilon'/\epsilon''$ . When terms in  $\mu^2 B^2$  are not neglected the ellipticity is found to exhibit a node at

$$\mu^2 B^2 \approx \omega^2 \tau^2 + 2\omega\tau - 1. \quad (14)$$

The case of *large*  $\mu B$  is not treated in this section since in general the loss tangent will decrease below unity. Thus in most cases the formulas developed above in the section give an approximate description.

Figure 5 displays the computer results using the exact equations (2), (3), and (5) as a function of  $\omega\tau$ . Evidently, the Faraday ellipticity can be of special interest: It depends strongly upon the collision time, even when  $\omega\tau < 1$ .

#### Anisotropy of the Effective Mass

Rau and Caspari have shown that, for the magnetic field along the [100] axis in *n*-type germanium, the  $m^*$  anisotropy is taken into account at small magnetic fields by using the Hall mobility  $\mu_H$  instead of  $\mu$  in the linear  $\mu B$  terms of Eq. (2). This statement can be extended to the Faraday effect in *n*-type silicon with the magnetic field applied along the [111] directions.<sup>5</sup>

For the magnetic field along the [100] and the [110] directions in *n*-type silicon, the solution is more complicated. However, in the limiting condition of  $\omega\tau < 1$  and  $\mu B < 1$ , it can be shown that the substitution of  $\mu_H$  for  $\mu$  in Eqs. (6) and (7) again correctly accounts for the anisotropy of  $m^*$ .

At high magnetic fields such that  $\mu B$  is larger than

both 1 and  $\omega\tau$ , the effect of anisotropy on the *rotation* disappears and  $\mu$  in Eq. (8) becomes equal to the conductivity mobility  $q\tau/m^*$  for all three crystallographic orientations.

Under the condition of cyclotron resonance,  $\omega\tau > 1$ , the effective mass anisotropy is clearly manifest. Some details for this region of high  $\mu B$  and  $\omega\tau$  have been recently published by Gurevich and Ipatova,<sup>6</sup> whose equations in the classical limit agree with the authors' calculation.

Anisotropy will also affect somewhat the value of  $\mu B(\theta_{\max})$  discussed above. For example, for the [111] orientation in silicon and the [100] orientation in germanium, the quantity  $\mu$  in Eq. (9) is to be replaced by  $(\mu\mu_H)^{1/2}$ .

The effect of the  $m^*$  anisotropy on the *ellipticity* is quite important in the limit when  $\mu B$  is much larger than 1 and  $\omega\tau$ . For example, when  $B$  is applied along a [111] axis,  $\mu^3$  must be replaced by  $\mu^2\mu_H$ .

So far, only the ellipticity arising from the difference in absorption of the two circularly polarized components of an incident wave has been considered. However, in crystals with the silicon or the germanium type anisotropy, the separation into two circular vibrations traveling along a longitudinal magnetic field is meaningful only when the field is applied along either the [111] or the [100] direction.<sup>5</sup> For other field orientations the

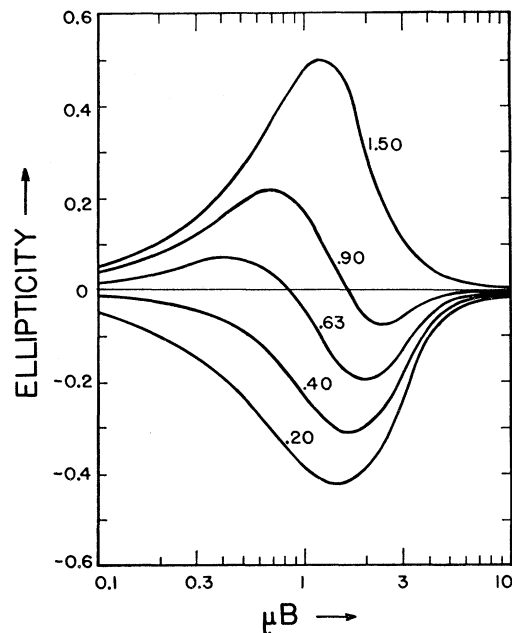


FIG. 5. Ellipticity as a function of  $\mu B$  at 35 kMc/sec in materials of relatively high conductivity. The curves are calculated with Eqs. (2) to (5), using  $\epsilon_{si}'/\epsilon_0=16$ ,  $\sigma=120$  ohm $^{-1}$  m $^{-1}$ ,  $l=0.5$  mm, and the values of  $\omega\tau$  as indicated in the graph. At low fields the sign is essentially determined by  $(\omega^2\tau^2 + 2\omega\tau - 1)$ , at high fields by  $(4\omega\tau - \sigma/\omega\epsilon_{si}')$ .

<sup>5</sup> B. Lax and L. M. Roth, Phys. Rev. **98**, 549 (1955).

<sup>6</sup> L. E. Gurevich and I. P. Ipatova, Zhur. Eksp. i Theoret. Fiz. **37**, 1324 (1959) [translation: Soviet Phys.-JETP **10**, 943 (1960)].

wave must be considered split into two elliptically polarized components, each propagating with its own velocity. The resultant ellipticity caused by the phase change will lead to a behavior similar to Faraday rotation. The effect of imperfect alignment of the field with the [100] or the [111] axis should be examined in this connection. Likewise, the outside shape of the sample is important: It may affect the mode of propagation, as well as introduce anisotropy in the depolarization coefficient if the sample is not perfectly circular.

### C. ROTATION

The experimental arrangement for 3-cm waves is shown in Fig. 6. A Varian X-13 klystron is tuned at 9.6 kMc/sec. The waveguide dimension (22-mm I.D.) is beyond cutoff for all modes but the propagated  $TE_{11}$ . The samples are in the form of disks of 0.5 to 0.9mm thickness and 21 mm in diameter, so that, placed inside a waveguide section, the sample fills practically the entire transverse guide area, but does not touch the guide wall. The magnet has hollow polepieces to accommodate the waveguide. Its field strength can be varied up to 0.4 v-sec/m<sup>2</sup> (4 kilogauss).

The detecting probes are mounted on a waveguide section free to rotate inside the magnet. Two methods of angle measurement can be used:

(a) With the electric field intensity inside a cylindrical guide proportional to  $\cos\phi$ , the terminal voltage of a probe using a "square-law" crystal rectifier will vary as  $\cos^2\phi$ . Here  $\phi$  is the angle between the probe position and the plane of polarization. When  $\phi = 45^\circ$ , the probe is in a practically linear portion of the  $\cos^2\phi$  distribution, which region is also most sensitive to the rotation. This permits one to express rotation in radians as

$$\theta = (i - i_B) / 2i,$$

where  $i_B$  and  $i$  are the currents through the galvanometer, with and without magnetic field, respectively. This method has been previously described by Allen.<sup>7</sup>

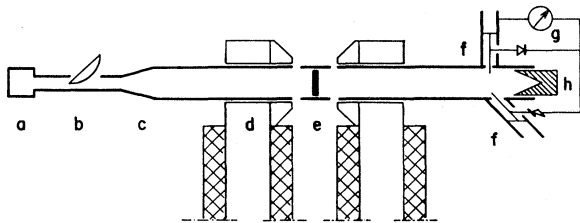


FIG. 6. Apparatus used for measuring the Faraday rotation at 9.6 kMc/sec: *a*, klystron; *b*, attenuator; *c*, rectangular-to-cylindrical waveguide transition; *d*, magnet with hollow polepieces; *e*, waveguide section containing sample; *f*, detecting probes; *g*, galvanometer measuring the difference in probe currents; *h*, termination. The entire right-hand section is free to rotate in the magnet.

<sup>7</sup> P. J. Allen, Rev. Sci. Instr. 25, 394 (1954).

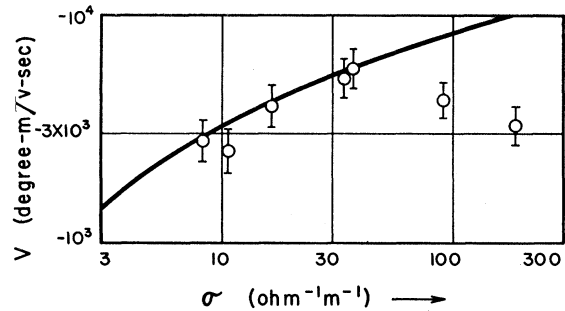


FIG. 7. Verdet constant  $V$  for *n*-type silicon at room temperature and 9.6 kMc/sec as a function of the conductivity  $\sigma$ . Experimental points and theoretical values are indicated by the circles and the solid curve, respectively. The (–) sign indicates that rotation due to electrons is negative, i.e., clockwise when the waves propagate in the direction of the magnetic field and the observer looks toward the source.

(b) If two oppositely connected probes (as shown in Fig. 6) are used, each at  $45^\circ$  on either side of the plane of polarization, and the system is balanced at  $B=0$ , a very high sensitivity to Faraday rotation can be obtained. This method requires well-matched crystals and calibration, but it does not assume a  $\cos^2\phi$  distribution. Moreover, certain variations in transmission, such as those associated with magnetoresistance, cancel out. This procedure, as well as the magnet used in the X-band experiment, have been previously described by one of us.<sup>8</sup> Measurements by both methods agreed within 5%.

A similar arrangement was constructed for the 35-kMc/sec experiment. In order to increase the observable effect and to find nonlinearities in the  $\theta$  vs  $B$  behavior, a 7-inch Diecraft magnet was used. Magnetic fields up to 2 v-sec/m<sup>2</sup> (20 kilogauss) were attained, with a uniformity of 2% over the useful region.

The samples, chosen larger than the waveguide cross section, were supported between two sections of the guide pushed towards each other. This sample-to-waveguide contact should diminish depolarization effects.

The rotating section of the guide is terminated by a 1N26 crystal in a tuned "stub." This detector is rotated, and a plot of the power distribution of the  $TE_{11}$  mode vs angle near the minimum is obtained. An X-Y recorder is very convenient for this purpose, with the Y axis activated by the crystal detector signal, and the X axis connected to a potentiometer measuring the angular position of the detector. At high power levels the minimum can be made very sharp.

For measurements at liquid nitrogen temperature, the sample is tightly held between two thick-walled waveguide sections. The sections are in good thermal contact with the metal wall of a special container filled with liquid nitrogen. When well insulated from the rest of the apparatus, a thermocouple showed this to be sufficient for cooling the sample to 78°K, with a possible

<sup>8</sup> S. Broersma, Am. J. Phys. 24, 500 (1956).

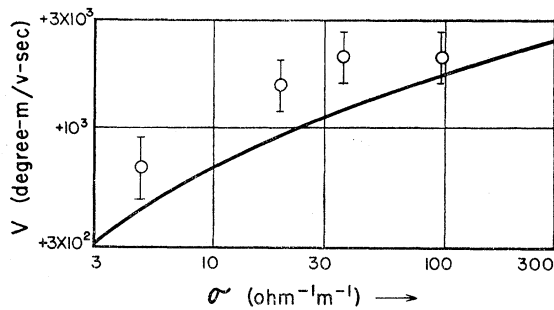


FIG. 8. Verdet Constant  $V$  for  $p$ -type silicon at room temperature and 9.6 kMc/sec as a function of the conductivity  $\sigma$ . The (+) sign indicates that the rotation due to the holes is positive.

error of  $4^\circ$ . Polystyrene plugs are used to guide the power through the space between the sample holder and the rest of the waveguide circuit.

Standing waves, which are likely to arise due to reflections at waveguide discontinuities, sample faces and termination, may lead to serious error. It was noted that, as the sample position is varied along the tube, deviations as high as  $\pm 20\%$  in the value of the rotation can show up. The variation follows a "standing wave pattern." To correct this, the reflections were reduced by matching the impedance at the sample surface with quarter-wavelength sections of a suitable dielectric.<sup>9</sup> The error limits given in the graphs are determined primarily by the variation of  $\theta$  due to standing wave effects.

#### Silicon at 300°K with 10 kMc/sec

Single crystals of silicon doped with arsenic and boron, in the resistivity range from 40 to 0.5 ohm-cm at 300°K were investigated. The corresponding impurity concentrations are:  $N_d \approx 2 \times 10^{14}$  to  $8 \times 10^{15}$  and  $N_a \approx 7 \times 10^{14}$  to  $4 \times 10^{16}$  per  $\text{cm}^3$ . The samples were in the form of disks 21 mm in diameter, with faces in (100) planes. The magnetic field was applied in the [100] direction. The average thickness of the  $n$ - and the  $p$ -type samples was 0.85 and 0.50 mm, respectively.

The results are plotted in Figs. 7 and 8. The solid curves represent the calculations with an IBM-650 digital computer, using Eqs. (2) to (4). The value of  $\sigma$  for each sample was measured at room temperature with a four-point probe, and the associated values of  $\mu_H$  were taken from published data.<sup>10</sup> The cyclotron resonance value<sup>11</sup> of  $m^*$  was used to calculate  $\tau$ , and  $\epsilon_{st}/\epsilon_0$  was taken as 12. We corrected the experimental points with the factor 0.84 for guided waves.

We checked the proportionality of experimentally observed rotations with the thickness and with the magnetic field. The rotation differed 15% from a direct

proportionality with  $t$  when two or three slices were stacked together. This is probably due to standing waves and reflections at the multiple interfaces. Proportionality with the magnetic field was confirmed to within 3% in the working range of  $B$  (0 to 0.4 v-sec/ $\text{m}^2$ ). It is therefore meaningful to define a Verdet constant  $V = \theta/Bt$  for this experimental range.

It is noted from Fig. 7 that for low  $\sigma$  (up to 40  $\text{ohm}^{-1} \text{m}^{-1}$ ) the results for  $n$ -type silicon show good agreement with the calculated curve. The results for  $p$ -type silicon in Fig. 8 are systematically higher than the corresponding theoretical points, by a roughly constant factor of 1.7. This factor is close to the ratio of the conductivity mobility and the Hall mobility.

As Fig. 7 shows, the Verdet constant tends to drop for samples of higher conductivity. Very likely, this decrease in rotation is caused by plasma depolarization effects. Because the degree of capacitive and resistive coupling of the sample to the guide is not known, it is difficult to estimate the effective depolarization coefficient.

It is possible that this depolarization effect is responsible for the absence of a detectable Faraday rotation (as well as cyclotron resonance<sup>12</sup>) in gray tin. The free carrier concentration in this material exceeded  $10^{17}$  per  $\text{cm}^3$  in the available samples, so that plasma effects can easily dominate.

#### Silicon at 300°K with 35 kMc/sec

Room-temperature rotation was also measured at 35 kMc/sec using fields as high as 2 v-sec/ $\text{m}^2$ . In Fig. 9

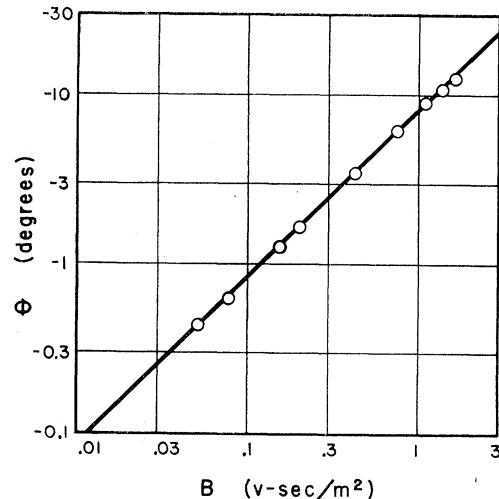


FIG. 9. Rotation as a function of the magnetic field  $B$  for a typical silicon sample ( $n$  type,  $\sigma \approx 30 \text{ ohm}^{-1} \text{m}^{-1}$ ,  $t = 0.85 \text{ mm}$ ) at room temperature and 35 kMc/sec. The slope of the straight line is 1, hence a Verdet constant can be defined.

<sup>9</sup> A. B. Bronwell and R. E. Beam, *Theory and Application of Microwaves* (McGraw-Hill Book Company, Inc., New York, 1947), p. 278.

<sup>10</sup> F. J. Morin and J. P. Maita, *Phys. Rev.* **96**, 28 (1954).

<sup>11</sup> G. Dresselhaus, A. F. Kip, and C. Kittel, *Phys. Rev.* **98**, 368 (1955).

<sup>12</sup> This was investigated in cooperation with Dr. R. N. Dexter of the Physics Department, University of Wisconsin. Runs were made with a series of single-crystal samples at liquid helium temperatures. A very slight photosensitivity as well as the presence of plasma effects were noted in some samples, but cyclotron resonance was not observed.

a typical  $\theta$  vs  $B$  curve, obtained for an  $n$ -type  $30 \text{ ohm}^{-1} \text{ m}^{-1}$  sample, is given, clearly showing the proportionality of the rotation to the magnetic field.

The measured Verdet constants for  $n$ - and  $p$ -type crystals are presented in Figs. 10 and 11, respectively. For the  $n$ -type samples the agreement with the theory is entirely satisfactory. There is no deviation in the high conductivity range. Very likely depolarization effects are absent here for the following reasons: A good physical sample-to-waveguide contact is obtained: The sample extends well beyond the waveguide walls appearing as an "infinite" sample to the guided waves. Furthermore, the ratio  $\omega_p^2/\omega^2$  (where  $\omega_p$  is the plasma frequency) on which the magnitude of the depolarization effect depends, is lower now than in the  $X$ -band experiment by a factor of 13.

As in the case of  $X$ -band measurements, the Verdet constants of the  $p$ -type material lie systematically above the theoretical curve, which is calculated using the Hall mobility in Eqs. (2) to (4). The ratio of the

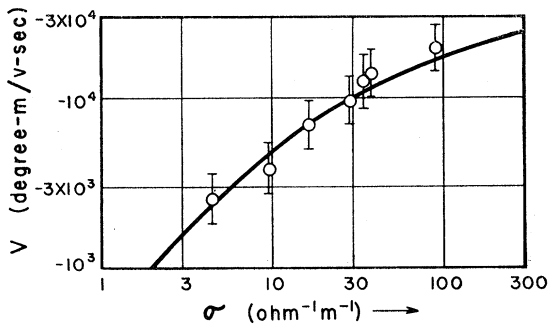


FIG. 10. Verdet constant  $V$  for  $n$ -type silicon at room temperature and 35 kMc/sec as a function of the conductivity  $\sigma$ . Experimental points and theoretical values are indicated by the circles and the solid curve, respectively.

experimental and the theoretical values is roughly a constant, 1.5, for the investigated conductivity range.

**Silicon at 78°K with 35 kMc/sec**

Preliminary measurements of the rotation were made at 78°K in  $n$ - and  $p$ -type crystals of silicon. Figure 12 gives experimental points as a function of the magnetic field. The  $n$ -type sample ( $\sigma_{78} \approx 30 \text{ ohm}^{-1} \text{ m}^{-1}$ ) shows a maximum in the  $\theta$  vs  $B$  curve at  $0.9 \text{ v-sec/m}^2$ . This indicates a mobility of about  $1.4 \text{ m}^2/\text{v-sec}$ , which is somewhat larger than expected at this temperature, viz., 1.1 to  $1.2 \text{ m}^2/\text{v-sec}$ . The  $p$ -type sample ( $\sigma_{78} \approx 40 \text{ ohm}^{-1} \text{ m}^{-1}$ ) shows no maximum in the available range of magnetic fields suggesting a mobility lower than  $0.9 \text{ m}^2/\text{v-sec}$ . This is in agreement with the corresponding dc data.

**Germanium at 78°K with 35 kMc/sec**

In germanium, it was possible to attain much higher values of  $\mu B$  at 78°K. This material was therefore used

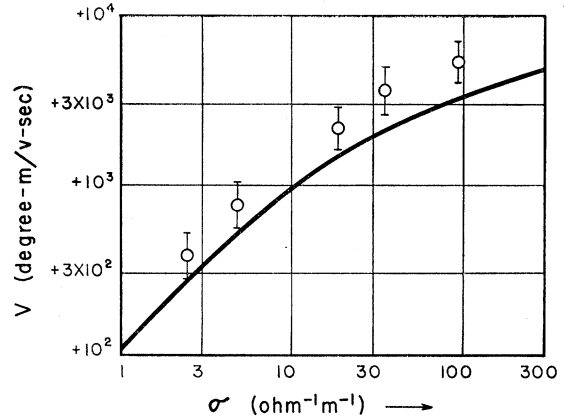


FIG. 11. Verdet constant  $V$  for  $p$ -type silicon at room temperature and 35 kMc/sec as a function of the conductivity  $\sigma$ .

to study the effect of high magnetic fields on the rotation.

Two  $n$ -type germanium crystals were examined at 78°K and 35 kMc/sec. The sample thickness was 0.5 mm. The disks were cut somewhat larger than the inside diameter of the waveguide, and were clamped tightly by two waveguide sections pushed together. The magnetic field was applied along a  $[100]$  axis. The room-temperature conductivity of the two crystals, indicated as samples  $A$  and  $B$  in Fig. 13, was  $4 \text{ ohm}^{-1} \text{ m}^{-1}$  and  $18 \text{ ohm}^{-1} \text{ m}^{-1}$ , respectively. On the basis of this the parameters for 78°K were extrapolated from published data,<sup>13</sup> viz.,  $22 \text{ ohm}^{-1} \text{ m}^{-1}$  and  $120 \text{ ohm}^{-1} \text{ m}^{-1}$  for the conductivity, and  $3.5 \text{ m}^2/\text{v-sec}$  and  $3.0 \text{ m}^2/\text{v-sec}$  for the Hall mobility of the two samples, respectively. The collision time was estimated from the mobility

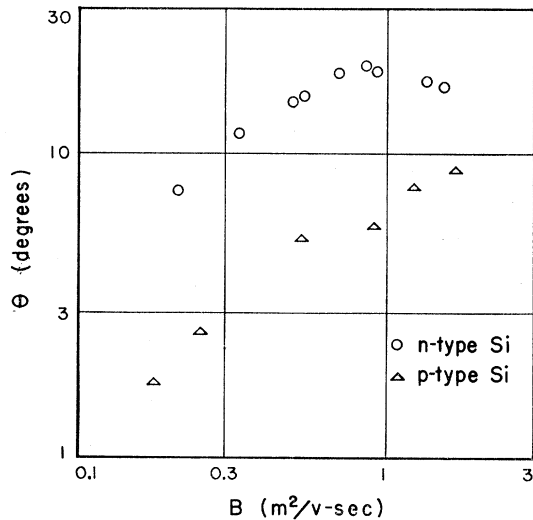


FIG. 12. Rotation at 78°K and 35 kMc/sec as a function of the magnetic field  $B$ , for  $n$ - and  $p$ -type silicon with  $\sigma = 30$  and  $40 \text{ ohm}^{-1} \text{ m}^{-1}$ , respectively, and  $l \approx 1 \text{ mm}$ .

<sup>13</sup> P. P. Debye and E. M. Conwell, Phys. Rev. 93, 693 (1954).

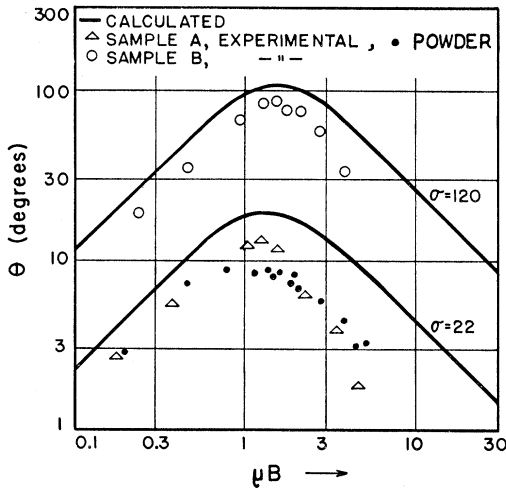


FIG. 13. Rotation as a function of  $\mu B$  for  $n$ -type germanium at 78°K and 35 kMc/sec. The solid curves are calculated with Eqs. (2) to (4), using  $\epsilon_{st}'/\epsilon_0=16$ ;  $\sigma=22(A)$  and 120( $B$ )  $\text{ohm}^{-1} \text{m}^{-1}$ ;  $\mu=3.5$  and  $3.0 \text{ m}^2/\text{v}\text{-sec}$ ; and  $\omega\tau=0.63$  and  $0.55$ , respectively. Sample  $A$  was measured both as a single crystal and as a powder. The crystal rotations for  $A$  and  $B$  refer to a thickness of 1 mm. The powder rotation was made equal to this for the lowest magnetic field.

and the cyclotron resonance effective mass.<sup>11</sup> This gave the values of 0.63 and 0.55 for  $\omega\tau$  of samples  $A$  and  $B$ , respectively. The dielectric constant of the host material,  $\epsilon_{st}'/\epsilon_0$ , was taken equal to 16. With these values the theoretical curves were computed.

The calculated curves and the experimental points are plotted in Fig. 13. Evidently, the experimental results exhibit the rotation maxima discussed before. These occur at values of  $\mu B$  which lie within a few percent of those calculated.

In both cases the magnitude of the rotation is considerably below the theoretical curves. There are several effects which may cause this: (a) The calculation assumes that the conductivity is due entirely to electrons, the opposing contribution of the holes to the rotation being neglected. In particular, if the minority carrier mobility is smaller than that of the majority carriers, this effect can be strong at high magnetic fields. (b) In the range where  $\omega\tau$  approaches 1, the rotation becomes rather sensitive to this parameter. Lower values of  $\theta$  thus may indicate a larger value of  $\tau$  than has been estimated for both crystals. The measurements of the Faraday ellipticity for the same samples, also show a better fit when assuming a larger value for  $\tau$ . (c) In connection with the large polarizability of the un-ionized impurity electron orbits, the value of  $\epsilon_{st}'$  can be larger than at room temperature. If this is taken into account, the theoretical line becomes again somewhat lower, especially at high magnetic fields. (d) Finally, it is possible that depolarization effects have not been eliminated entirely.

Measurements were also performed on the purer of the germanium samples ( $A$ ) after it had been powdered

(see Fig. 13). The maximum occurs at the same field strength as that for the single crystal, but for the powder it appears broader. We normalized the powder rotations to the same effective thickness as the single crystal by making both curves coincide at the lowest magnetic field. The relative widths of the maxima can be caused by randomness of the particle orientations, since the position of the maximum depends somewhat upon the direction of the magnetic field with respect to the crystallographic axes.

#### D. ELLIPTICITY

The 1N26 crystal, mounted in the probe, was calibrated by plotting the field pattern of the  $TE_{11}$  mode in the guide. Since the current vs angle plot showed a cosine-square dependence, the detector was assumed to measure the square of the electric field. In that case the ellipticity equals

$$E = (i_{\min}/i_{\max})^{\frac{1}{2}},$$

where  $i$  is the observed current in the detector circuit for the position of the minimum and the maximum of the electric field, respectively.

Even with the magnetic field off, there usually existed a detectable ellipticity ( $E_0$ ), caused by circuit imperfections. This was minimized by rotating a dielectric plate, placed in the waveguide parallel to the axis, or by gently squeezing the guide, until the signal at the minimum was below the amplifier noise. Each Faraday ellipticity reading was checked by repeating it with reversed magnetic field. When  $E_0$  was adequately minimized, the magnitude of both readings was equal. The two measurements should in general differ by  $2E_0$ .

The following experiment was used to check that the measured ellipticity indeed is an odd function of the

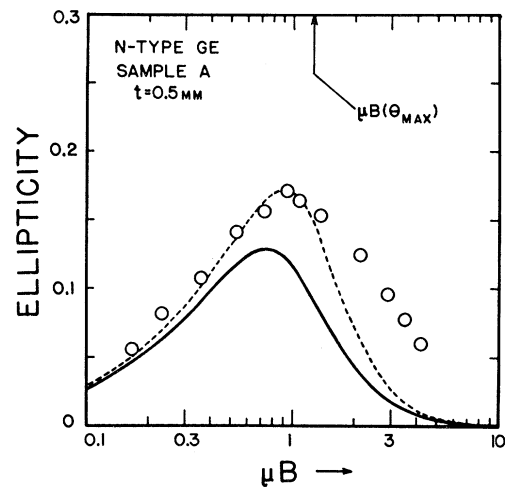


FIG. 14. Observed and calculated ellipticity vs  $\mu B$  for  $n$ -type Ge (sample  $A$ ) at 78°K and 35 kMc/sec. The solid curve is calculated with Eqs. (2) to (5), using  $\epsilon_{st}'/\epsilon_0=16$ ,  $\sigma(78^\circ)=22 \text{ ohm}^{-1} \text{m}^{-1}$ , and  $\omega\tau(78^\circ)=0.63$ . The abscissa is obtained using  $\mu(78^\circ)=3.5 \text{ m}^2/\text{v}\text{-sec}$ . The dotted curve is based on  $\omega\tau=0.90$ .

magnetic field. An initial ellipticity  $E_0$  was purposely introduced by inserting a dielectric plate in the wave guide on the klystron side of the apparatus, at an arbitrary angle  $\phi$  with the plane of polarization. It was then observed that the ellipticity increased for one magnetic field direction, and decreased for the opposite field direction. The effects for the two field orientations interchanged when the dielectric plate was rotated to the  $-\phi$  position, i.e., when the sign of  $E_0$  was reversed.

#### Germanium at 78°K with 35 kMc/sec

Absolute values of the Faraday ellipticity were measured at 78°K and 35 kMc/sec on the two *n*-type germanium samples, *A* and *B*. The purer sample, *A*, showed the behavior characteristic of a low-loss material. In Fig. 14 the observed and calculated ellipticity are plotted as a function of the magnetic field. The experimental points exhibit a maximum near  $\mu B=1$ , similar to that shown by the Faraday rotation. The magnitude of the measured ellipticity is somewhat larger than the calculated values. It is quite possible that the value of the effective collision time, obtained from the relation  $\tau = \mu m^*/q$ , which gives  $\omega\tau=0.63$  for sample *A*, should be larger. The value of 0.9 for  $\omega\tau$  gives a better fit as is shown in Fig. 14 with the dashed line.

The results obtained for sample *B* are given in Fig. 15. The crystal displays qualitatively the behavior expected for lossy samples. In particular, a change of sign is observed as the magnetic field is varied. A closer fit can be obtained with a larger collision time  $\tau$  and a smaller  $\sigma/\omega\epsilon_{st}'$ . As pointed out for the rotation it is possible that the effective conductivity  $\sigma$  is smaller than the corresponding dc value and also that  $\epsilon_{st}'$  is somewhat larger.

#### Germanium and Silicon at 300°K

Some preliminary measurements of the Faraday ellipticity were carried out at room temperature with fields up to 2 v-sec/m<sup>2</sup>, for silicon and germanium samples having resistivities between 0.20 and 0.01 ohm-m. Because of the large power difference between the maximum and minimum readings, the detector calibration was not sufficiently precise to warrant a

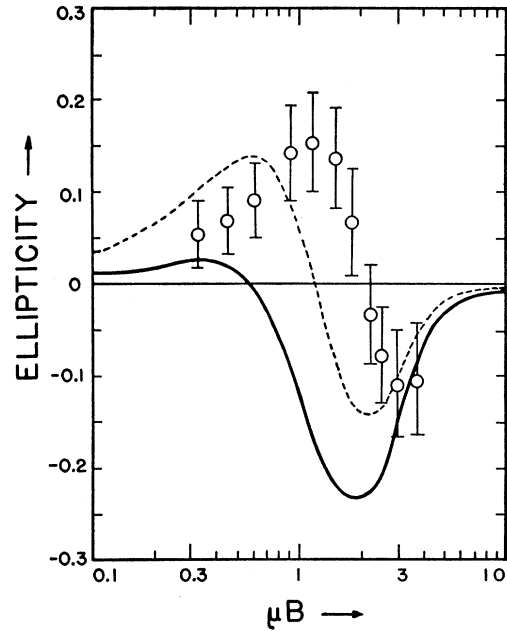


FIG. 15. Observed and calculated ellipticity as a function of  $\mu B$  for *n*-type Ge (sample *B*,  $t=0.5$  mm) at 78°K and 35 kMc/sec. The solid curve is calculated with Eqs. (2) to (5), using  $\epsilon_{st}'/\epsilon_0 = 16$ ,  $\sigma(78^\circ) = 120 \text{ ohm}^{-1} \text{ m}^{-1}$ , and  $\omega\tau(78^\circ) = 0.54$ . The abscissa is obtained using  $\mu(78^\circ) = 3.0 \text{ m}^2/\text{v-sec}$ . The dotted curve is obtained with  $\omega\tau = 0.75$ .

quantitative discussion. The effect was measurable and the observed values did not deviate by more than a factor of 2 from the calculated values. The measured ellipticity was proportional to the magnetic field, and it reversed sign when the field was reversed.

#### ACKNOWLEDGMENTS

The authors are indebted to Dr. M. Prince and Dr. J. R. Madigan of Hoffman Electronics Corporation for the generous supply of silicon crystals and to Mr. R. W. Berkstresser of Sylvania Electric Products for making d.c. conductivity measurements. We thank Professor A. W. Ewald for his valuable advice and for the single crystals of gray tin, Professor R. E. Beam and Professor M. E. Brodwin for the use of some of the microwave components and for germanium samples.